ELSEVIER

Catalysis Today 82 (2003) 67–74

CATALYSIS TODAY

www.elsevier.com/locate/cattod

Controlled Pt deposition in membrane mesoporous top layers

Denis Uzio, Sylvain Miachon, Jean-Alain Dalmon*

Institut de Recherches sur la Catalyse—CNRS, 2, av. Albert Einstein, 69626 Villeurbanne Cedex, France

Abstract

Different methods of platinum deposition in the porous framework of a tubular ceramic membrane have been investigated. Metal loading, localization, and dispersion were studied using electron microscopy techniques. Results shows the characteristics of the platinum deposit deeply depended on the membrane structure, Pt precursor nature, and application procedure.

Keywords: CMR; Mesoporous membrane; Platinum deposition

1. Introduction

Among the three different types of catalytic membrane reactors (CMR) [1], only the contactor-mode necessitates a catalytically active membrane. As a matter of fact, in most cases, the two other types of CMR, extractors, and distributors, combine a fixed-bed catalyst and a membrane that simply controls transfers.

Catalytically active membranes can either be intrinsically active or act as a support for an active phase. In this last case, the loading and the location of the catalyst in the membrane are of importance with respect to the final reactor performance and these parameters should be adapted as a function of the type of reaction, catalyst, and membrane.

In our group, we have developed the use of catalytic membrane contactors for gas–liquid applications [2,3], in the line of pioneering studies by Cini and Harold [4]. The idea was to take benefit from the unique structure of a catalytic membrane, when compared to a conventional catalyst. A comparative schematic of the two systems is given in Fig. 1. When a conventional catalyst presents only one way to enter and get out of the catalytic pore, the pore of a catalytic membrane shows two ways, corresponding to the two sides of the membrane wall. Therefore, immiscible reactants can be introduced separately from both sides of the catalytic membrane, a configuration that favors the contact between the two reactants and the catalyst [4].

By using this type of membrane reactor called interfacial contactor [1], in a gas–liquid reaction, it has been shown that the performance is not limited by the concentration of the gaseous reactant, as generally is the case in conventional reactors [2]. This observation that the interfacial contactor may favor the access to the catalyst of the reactant that limits the performance of conventional systems has also been demonstrated in other cases. For instance, when polar and non-polar species should react, the presence of a hydrophobic polymer membrane containing the hydrophilic catalyst favors the access of the non-polar reactant and greatly increases the performance [5,6]. Here also, position and loading of the active phase within the membrane wall play a major role [6].

* Corresponding author. Tel.: +33-4-7244-5368; fax: +33-4-7244-5399.
E-mail address: dalmon@catalyse.univ-lyon1.fr (J.-A. Dalmon).

0920-5861/$ – see front matter
doi:10.1016/S0920-5861(03)00203-7

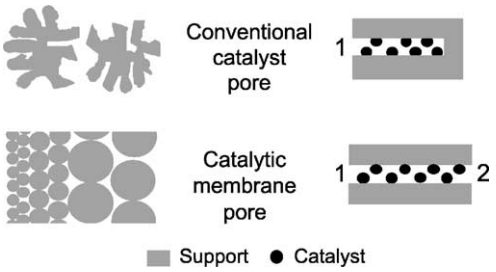

Fig. 1. Schematics of conventional catalyst and catalytic membrane pore structures.

In this paper, we report on different possibilities for a controlled deposition of an active metal (platinum) in the pores of a ceramic membrane.

2. Experimental

2.1. Materials

Commercial supports, from Pall-Exekia (PE-T1-70), have been used in this study. These are single tubes of ca. 10 mm OD, made of several concentric macroporous α-Al_2O_3 layers with decreasing pore size from external to internal sides. The final mesoporous γ-Al_2O_3 top layer is thus located inside the tube. The main characteristics of the supports used in this study are given in Table 1.

In most cases, a solution of hexachloroplatinic acid, H_2PtCl_6, has been used as platinum precursor. Some experiments have also been made using $Pt(NH_3)_4Cl_2$.

In all cases the tubular support is first dried at 180 °C. After weighing, it is dipped during 2 h in stirred water before Pt introduction.

Two deposition methods have been used, the first one, ionic impregnation, involving a stronger interaction with the support than the second, based on evaporation–crystallisation steps.

Table 1
Main characteristics of the Pall-Exekia T1-70 multilayered supports

Layer	Material	Thickness (μm)	Pore size (nm)
1	α-Al_2O_3	1500	12000
2	α-Al_2O_3	40	800
3	α-Al_2O_3	20	200
4	γ-Al_2O_3	3–4	5, 10, 25

2.1.1. Ionic impregnation

According to Ref. [7], the mechanism of Pt anchoring is an electrostatic interaction between hydroxyl groups of the support surface and Pt-containing ionic species. For instance, when H_2PtCl_6 was used, $[PtCl_6]^{2-}$ anions were fixed on OH_2^+ surface sites formed in acidic medium. An amount of 250 cm^3 of solution with 0.1 g Pt/l was used for tubes of 10 cm length. Two ways of impregnation have been used (Fig. 2). In the first one, the tubular support is simply dipped in the precursor solution (Fig. 2(A)). In the second, the ends of the tube are first tightly caped to allow the penetration of the precursor only from the larger pore (external) side of the support (Fig. 2(B)) to the top layer side.

The time of impregnation was varied between 1 and 20 h. The tubes were then washed by forcing a water flow through the porous tube with a pump, from the inner to the outer side (transmembrane flow ca. 0.1 ml/min). The samples were then dried under flowing nitrogen at 100 °C.

2.1.2. Evaporation–crystallization deposition

This method was based on the so-called “reservoir” method [8]. The tube was first dipped for 2 h in pure water and then for 5–10 h in an H_2PtCl_6 precursor solution (0.1–10 g Pt/l). The sample was then dried at room temperature by a stream of dry air flowing inside the tube, to favor evaporation from the inner side and deposition in the top layer.

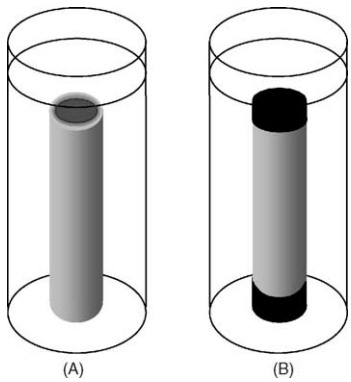

Fig. 2. Pt ionic impregnation of the tubular supports: mode A and mode B.

2.1.3. Platinum activation

Metallic platinum is obtained after thermal treatment of the sample under flowing hydrogen (1 °C/min up to 200 °C followed by 10 h plateau).

2.2. Characterization methods

Scanning electron microscopy (JEM 840 A) has been used to determine the position of platinum particles inside the porous structure of the multilayered ceramic material. Samples for crosswise Pt EDX analyses were prepared by breaking the tube and after depositing a C film on the section.

Transmission electron microscopy studies (JEM 2010) have been performed, either on powders prepared by scrapping the layers where SEM indicate the presence of Pt, or directly on the tubes following the method described in Ref. [9].

Gas permeation measurements were performed before and after Pt deposition using a conventional setup [10].

3. Results

3.1. Ionic impregnation method

3.1.1. Effect of the introduction mode

Figs. 3 and 4 give, for both modes, the result of the crosswise Pt EDX analysis (linescan) for a Pall-Exekia (PE) tube with a 5 nm pore size γ-Al_2O_3 top layer, after ionic impregnation with H_2PtCl_6.

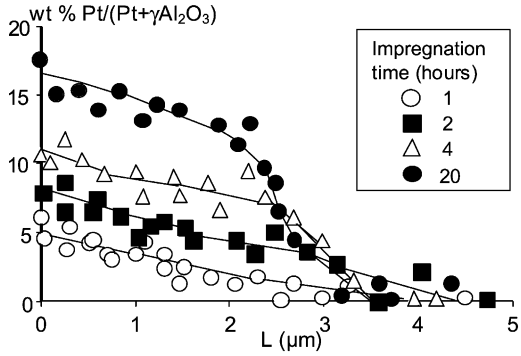

Fig. 3. Pt EDX radial analysis (L is the distance between the top layer surface and the position of the EDX probe). PE support with 5 nm pore size top layer: mode A (H_2PtCl_6).

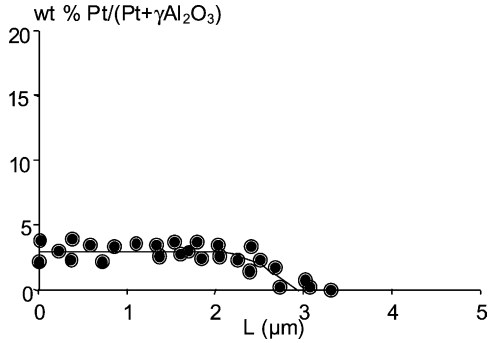

Fig. 4. Pt EDX radial analysis. PE support with 5 nm pore size top layer: mode B (H_2PtCl_6, 20 h).

Fig. 3 corresponds to the A introduction mode (see Fig. 2; 1–20 h of impregnation). For each impregnation time, experimental points correspond to several line scans, as obtained in different positions in the sample. In all cases, Pt deposition is restricted to the top layer, with a decreasing concentration profile from the external surface down to zero at the γ-Al_2O_3/α-Al_2O_3 boundary. Moreover, the longer the impregnation time, the higher the Pt loading.

Fig. 4 corresponds to the B introduction mode (20 h impregnation). Contrary to the result given in Fig. 3 for the same material, the radial Pt loading is constant, when mode B is used.

Fig. 5 is a typical TEM micrograph obtained with the powder scratched from the PE tube after the mode B impregnation. Pt particles are clearly visible. Fig. 6 gives the Pt particle size distributions obtained with impregnation modes A (left) and B (right).

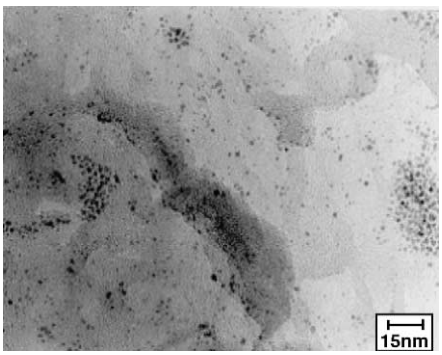

Fig. 5. TEM micrograph. PE tube (5 nm pore size top layer): mode B.

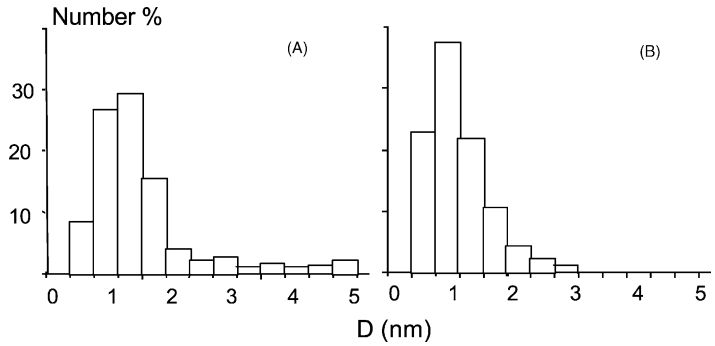

Fig. 6. Pt particle size distributions. PE tube (5 nm pore size top layer): modes A (left) and mode B (right).

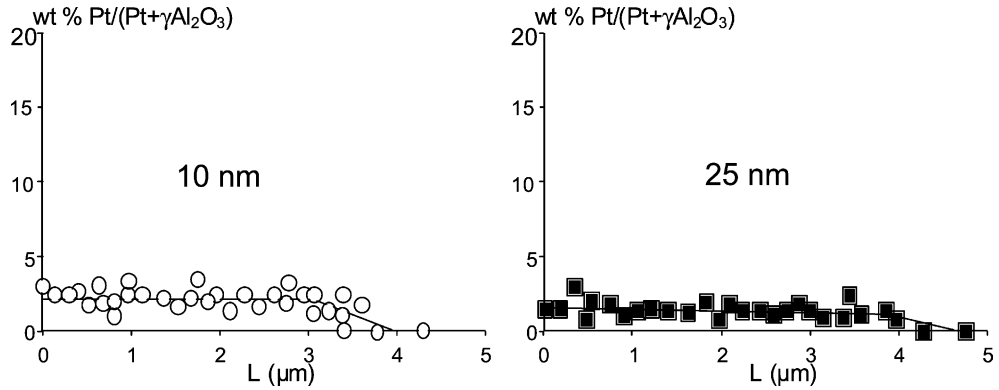

Fig. 7. Pt EDX radial analyses. PE supports, 10 nm (left) and 25 nm (right) pore size top layers: mode A (H_2PtCl_6, 20 h).

3.1.2. Effect of the top layer pore size

Fig. 7 shows crosswise Pt line scans obtained after mode A impregnation of PE γ-Al_2O_3 tubes with average top layer pore size of 10 and 25 nm (H_2PtCl_6, 20 h of impregnation). Contrary to the previous case (Fig. 3), the Pt loading appears constant in the thickness of the top layer when larger pore sizes are used with mode A.

3.1.3. Effect of the precursor nature

Fig. 8 shows the Pt loading obtained when $Pt(NH_3)_4Cl_2$ is used as precursor, with the same material and introduction mode as in Fig. 3. Contrary to H_2PtCl_6, the $Pt(NH_3)_4Cl_2$ precursor leads to a homogeneous profile within the 5 nm pore size top layer.

3.2. Evaporation–crystallisation deposition method

Fig. 9 gives the Pt loading profile after evaporation of a 10 g Pt/l solution (H_2PtCl_6) used to fill the porous volume of a PE tube (5 nm top layer). When compared to the ionic impregnation, the Pt distribution is not so homogeneous. High Pt loadings are observed, Pt being also present in the macroporous alumina sublayers of

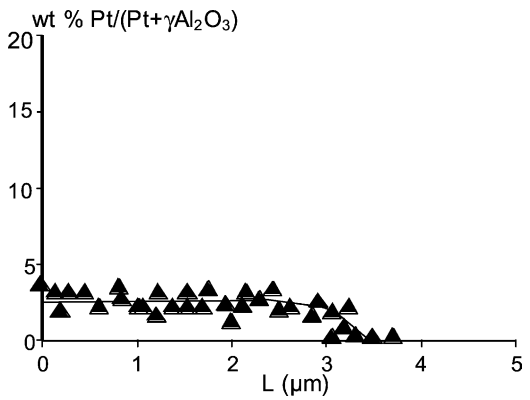

Fig. 8. Pt EDX radial analysis. PE support with 5 nm pore size top layer: mode A ($Pt(NH_3)_4Cl_2$, 20 h).

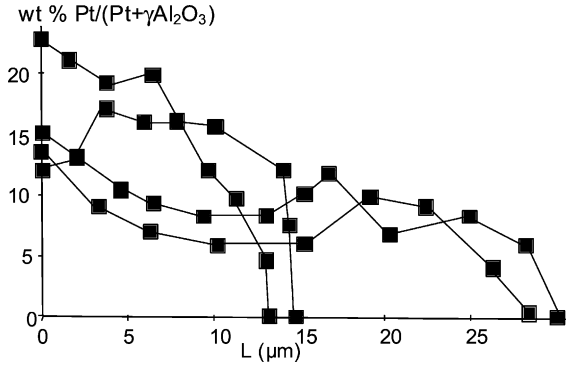

Fig. 9. Pt EDX radial analysis (the different lines correspond to different positions of the EDX analysis). PE support (5 nm pore size top layer). Evaporation method (H_2PtCl_6, 10 g Pt/l).

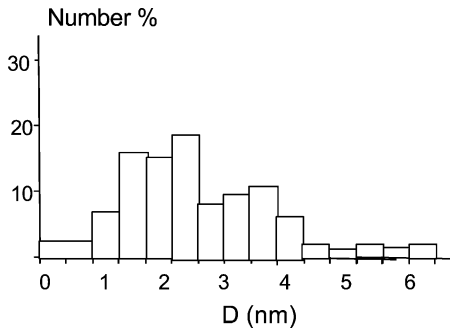

Fig. 10. Pt particle size distribution. PE tube (5 nm pore size top layer). Evaporation method.

the tube. Fig. 10 shows the Pt particle size distribution obtained in the material scratched from the tube. Large particles are observed, up to 7 nm.

4. Discussion

4.1. Ionic impregnation method

4.1.1. Effect of the introduction mode

Using the same material, the Pt loading profile is quite different according to the introduction mode (Figs. 3 and 4).

In mode A, the impregnation solution is in direct contact with the mesoporous top layer. This layer acts as a diffusion barrier for the Pt precursor species and originates a concentration polarization effect, leading to a Pt concentration profile decreasing from the external surface of the top layer (Fig. 3). During the washing step, the water flow is directed from the inner side to the outer side of the tube and has no or little effect to remove the Pt that has been accumulated in the mesopores. As shown in Fig. 3, the longer the time of impregnation, the higher is this effect of concentration polarization.

In some experiments, a dynamic impregnation has been performed, the precursor solution being forced to flow through the layers, from the inner side of the tube. For these conditions, the sieving effect of the top layer is emphasized and Pt surface concentration up to 70 wt.% can be obtained.

When the B mode is used, the only way for Pt species to enter in the mesoporous top layer is from the external side of the tube, i.e. through the macropores. Even if the concentration polarization effect may occur at the mesopore–macropore boundary, the washing step, directed in the right orientation, will remove the weakly bounded Pt species accumulated there. After the washing step, only remain the species interacting with the support. As a matter of fact, the final Pt loading, close to 3 wt.%, is in agreement with what can be expected from an anionic impregnation, according to the specific area of the γ-Al_2O_3 top layer (ca. 150 $m^2\,g^{-1}$). As shown in Fig. 4, the Pt concentration profile is then homogeneous and limited to the top layer, the ability of the α-Al_2O_3 sublayers to fix $[PtCl_6]^{2-}$ anions being very low.

As far as Pt particle size distributions are concerned (Fig. 6), both modes lead to distributions showing a maximum close to 1.5 nm. However, mode A originates some large particles (sizes up to 6 nm) that are likely produced by the high surface Pt loading due to the concentration polarization phenomenon. These large Pt particles are not numerous. But, Fig. 6 gives distributions in number and in weight, a particle of 6 nm is equivalent to 27 particles of 2 nm. Therefore, the high surface loadings observed in Fig. 3 will generate a limited number of very large particles.

4.1.2. Effect of the top layer pore size

When the top layer pore size increases, the mode A does not lead to decreasing Pt loading profiles, as was observed with the 5 nm pore size top layer. Fig. 7 indeed shows a constant Pt concentration in the 10 and 25 nm mesoporous pore size layers, with a

value roughly proportional to the specific area of the γ-Al_2O_3 layers (80 and 40 $m^2\,g^{-1}$, respectively).

Two factors may explain this change. The first one is linked to the diffusivity of Pt precursors in the pore. As a matter of fact, it has been reported [11] that there is a relation between the size of the diffusing species (here the Pt precursor), the pore size, and the diffusion coefficient in the pore. A simple calculation, using 0.45 nm for the size of the diffusing species (based on interatomic distances) shows that the diffusivity of the Pt precursor is about five times lower in the 5 nm pores than that in the 25 nm pores (where it is close to the molecular diffusion value). The second factor that may contribute to the observed change is that the dynamic washing through the pores is probably more efficient, when the pore size increases, to remove the Pt species that are weakly fixed to the top layer.

4.1.3. Effect of the precursor nature

Contrary to H_2PtCl_6, the $Pt(NH_3)_4Cl_2$ precursor leads to a homogeneous profile within the 5 nm pore size top layer, even when using mode A. This could be due to the planar structure of the cationic complex that could favor the diffusion of the precursor in the pores. Another, and probably important parameter, is that the impregnation is now performed in a basic medium, which may play a major role when polarization concentration phenomena are concerned.

4.2. Evaporation–crystallisation deposition method

In this method, the main parameter controlling the Pt deposition is the concentration of the precursor solution in the pore. Owing to the high capillary forces in the top layer, there is, during the solvent evaporation, a progressive displacement of the Pt species towards the inner side of the porous tube. When saturation occurs, there is precipitation of the solute over the whole wet volume of support. Further on, a continuous Pt deposition occurs, the loading increases gradually towards the inner surface of the tube, as the solution continues to evaporate. This process is considered more thoroughly below.

The localization of this first Pt deposition does not depend on the chemical nature of the layer, but is mainly related, for a given tube, to the initial concentration of the solution (this explains why Pt could be present in the sublayers, Fig. 9). As pores structure and connectivity are not homogeneous through the sample, the Pt profile may vary as a function of the location, as shown in Fig. 9. It seems however that the total amount of Pt deposited (i.e. the area under the profile) is more or less constant, in keeping with the above deposition mechanism. This area also fits the Pt amount corresponding to the precursor present in the support porous volume.

The Pt profile deposition has been modelized in one-dimension, taking the *total* cylindrical volume V as variable, in order to simplify calculations and presentation. This approach allows to take into account straightforwardly the variation of solid platinum concentration in the porous system.

The origin of volumes is the central axis of the membrane tube. The volume will be translated into depth values in order to compare to the EDX analysis when necessary. The notations V^* and C^* are related to free volumes in the membrane tube wall porosity (volumes and concentration of solutions for example). The two are related in the following way: $V^* = \rho(V - V_1)$, where V_1 is the volume of the tube lumen and ρ the porosity of the membrane wall, supposed constant over the wall thickness.

The volume where the saturation is reached is denoted V_s. It can be written as

$$V_s = V_1 + \frac{C_0^* V_0^*}{\rho C_s^*} \tag{1}$$

that is, a depth into the membrane wall of

$$d_s = R_s - R_1 = \sqrt{R_1^2 + \frac{C_0^* V_0^*}{\Pi h \rho C_s^*}} - R_1 \tag{2}$$

where C_0^* is the starting concentration of the precursor solution (mol/m^3); V_0^* the starting volume of the precursor solution (m^3); h the length of the tubular membrane (m); C_s^* the saturation concentration of the precursor (mol/m^3); R_1 the internal radius of the tubular membrane (m); R_s the radius of the volume V_s (m).

Below this value of volume, the solution continues to evaporate, precipitating progressively the precursor on the surface of the membrane pores. During this second stage, the concentration of the solution keeps constant, equal to the saturation concentration. If this precipitation process is considered step by step, one can write the amount dn_t (mol) of catalyst precursor

that is left by the evaporation of a volume of solution dV^* as

$$dn_t = -C_s^* \, dV^* = -\rho C_s^* \, dV \quad (3)$$

Therefore, the total amount of catalyst precipitated for a variable V at a certain moment of the process after reaching V_s is

$$n_t = \rho C_s^* (V_s - V) \quad (4)$$

At a given time of the evaporation process, corresponding to a volume V describing the liquid surface position ($V_1 < V < V_s$), the deposited amount n_t offers a profile in two parts. The first part, between V_1 and V is a plateau. Let us denote it as n. The second part, between V and V_s of the n_t profile is decreasing from n to 0. This second part is equal to the integration of the Pt particle concentration over the variable V between V and V_s. Moreover, at the variable V, the concentration C_{Pt} of solid Pt precursor is equal to the ratio $n/(V - V_1)$ with

$$n = n_t - \int_V^{V_s} C_{Pt} \, dx = \rho C_s^* (V_s - V) - \int_V^{V_s} C_{Pt} \, dx \quad (5)$$

By differentiation and taking into account the limit value $C = 0$ for $V = V_s$, one can obtain:

$$C_{Pt} = \rho C_s^* \ln \frac{V_s - V_1}{V - V_1} = \rho C_s^* \ln \frac{R_s^2 - R_1^2}{R^2 - R_1^2} \quad (6)$$

The EDX analysis is given in platinum loading (at.%), that can be expressed as

$$l_{Pt} = \frac{M_{Pt} C_{Pt}}{M_{Pt} C_{Pt} + (1 - \rho) d_{Al_2O_3}} \quad (7)$$

with M_{Pt} and $M_{Al_2O_3}$ being the molar mass of Pt and alumina, respectively. $C_{Al_2O_3}$ describes the spatial molar concentration of alumina.

In order to plot the profile from the model, the following values were used: $M_{Pt} = 195.09\,g/mol$, $M_{Al_2O_3} = 101.96\,g/mol$, $d_{Al_2O_3} = 3900000\,g/m^3$, $R_1 = 0.34 \times 10^{-2}\,m$, $h = 0.1\,m$, $\rho = 0.35$, $V_0^* = 1.48 \times 10^{-6}\,m^3$, $C_0^* = 10\,g\ Pt/l = 51.26\,mol/m^3$, $C_s^* = 1740\,mol/m^3$ [12].

Therefore, depth of the first platinum deposition can be calculated to $d_s = 58\,\mu m$, i.e. $R_s = 0.3458 \times 10^{-2}\,m$. This value is higher than that experimentally observed by SEM–EDX (15–30 μm, Fig. 9). However, it should be noticed that there is some imprecision on the value used for C_s^*. As a matter of fact, this saturation concentration was obtained by adding hexachloroplatinic acid in the solution till insolubility was observed, which should deeply depend on the experimental conditions. On the other hand, there are certainly some dead-end pores that may trap a part of the Pt solution before precipitation starts. In comparison to what is used in the modeling, such phenomena will lower the Pt concentration of the solution, and therefore lower d_s.

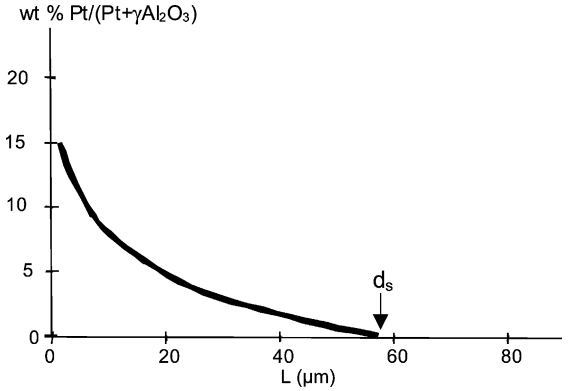

Fig. 11. Metal radial loading profile, as predicted from the model.

Fig. 11 gives a Pt profile, as obtained from the model. Taking into account the uncertainty for d_s, the agreement with the SEM–EDX data (Fig. 9) is rather good, especially concerning the shape of the deposition profile and the average loading (both modeling and experiments give a loading in keeping with that deduced from the precursor solution in the porous volume of the tubular support).

As far as the Pt particles size distribution is concerned (Fig. 10), there is an important number of large particles. This is likely due to the high Pt loading and also probably to the weak interaction that exists between the Pt precursor species and the support.

5. Conclusion

The specific geometry of a porous tubular membrane creates a series of possibilities for a controlled deposition of an active phase in the material. Parameters such as the mode of catalyst precursor

introduction, its nature, combined with the porous structure of the layers, may affect the final result in terms of loading, position, and dispersion of the active phase. All these characteristics of the catalytic membrane are of prime importance, when the performance of the CMR is considered.

Acknowledgements

The authors wish to express their acknowledgements to the European Commission, who funded this work through the programs Brite CT91 0406 and "WaterCatox", EVK1-CT-2000-00073.

References

[1] S. Mota, S. Miachon, J.-C. Volta, J.-A. Dalmon, Catal. Today 67 (2001) 169.
[2] J. Peureux, M. Torres, H. Mozzanega, A. Giroir-Fendler, J.-A. Dalmon, Catal. Today 25 (3–4) (1995) 409.
[3] S. Miachon, V. Perez, G. Crehan, E. Torp, H. Ræder, R. Bredesen, J.-A. Dalmon, Catal. Today 82 (2003) 75.
[4] P. Cini, M.P. Harold, AIChE J. 37-7 (1991) 997.
[5] I.F.J. Vankelecom, R.F. Parton, M.J.A. Casselman, J.B. Uytterhoeven, P.A. Jacobs, J. Catal. 163 (1996) 457.
[6] S. Wu, J.-E. Gallot, M. Bousmima, C. Bouchard, S. Kaliaguine, Catal. Today 56 (2000) 113.
[7] M. Che, O. Clause, C. Marcilly, Handbook of Heterogeneous Catalysis, in: Ertl, Knözinger, Weitkamp (Eds.), VCH, Weinheim, 1997, Chapter 2.2, p. 191.
[8] V.T. Zaspalis, W. van Praag, K. Keizer, J.G. van Ommen, J.H.R. Ross, A.J. Burggraaf, Appl. Catal. 74 (1991) 205.
[9] V. Perez, S. Miachon, J-A. Dalmon, R. Bredesen, G. Pettersen, H. Ræder, C. Simon, Separ. Purif. Technol. 25 (2001) 33.
[10] D. Uzio, J. Peureux, M. Torres, A. Giroir-Fendler, J. Ramsay, J.-A. Dalmon, Appl. Catal. 96-1 (1993) 83.
[11] H. Brenner, L.J. Gaydos, J. Colloid Interf. Sci. 58 (1977) 312.
[12] R. Becht, Information from Internal Johnson Matthey technical database, 2002, Personnal communication.